21st Australasian Fluid Mechanics Conference
Adelaide, Australia
10-13 December 2018

Large-eddy simulation of flow about a rotating cylinder at large Reynolds number

D. Pullin[1], **W. Cheng**[2] **and R. Samtaney**[2]

[1]Graduate Aerospace Laboratories, California Institute of Technology, Pasadena CA 91125, USA.

[2]Mechanical Engineering, Physical Sciences and Engineering Division, King Abdullah University of Science and Technology Thuwal, Saudi Arabia.

Abstract

Wall-resolved large-eddy simulations (LES) of flow past a rotating cylinder are described. The principal flow parameters are the dimensionless rotation speed $\alpha = \Omega D/(2U_\infty)$ and the Reynolds number $Re_D = U_\infty D/\nu$. We vary Re_D at fixed $\alpha = 0.6$ with emphasis on the lift-crisis phenomenon where, with increasing Re_D, the lift coefficient C_L decreases suddenly as Re_D passes though a narrow, critical band. Calculations of C_L and C_D are compared with experimental measurements to demonstrate that the lift crisis is captured by the LES. Results show that the mechanisms that drive the lift crisis when varying Re_D at fixed α are similar to those observed when varying α at fixed Re_D. Both data sets support a hypothesis which interprets the lift crisis as the result of near-wall, small-scale reversal flows aggregating into a relatively narrow zone, producing small-scale incoherent separation accompanied by a deep pressure minimum. Scaling of the skin friction coefficient with $Re_D^{1/2}$, which was found previously for flow past a non-rotating, is also observed for $\alpha = 0.6$.

Introduction

The drag crisis for flow over a stationary, non-rotating cylinder is well known. This is characterized by a sudden decrease in the drag coefficient C_D when the Reynolds number $Re_D = U_\infty D/\nu$ (D is the cylinder diameter, U_∞ the free-stream speed and ν the kinematic viscosity) increases from subcritical to supercritical values over a range of approximately $Re_D = 2\times10^5 - 4\times10^5$. Lehmkuhl *et al.* [1] used LES to detect a mean-flow separation bubble upstream of the primary separation zone at supercritical Re_D. The detailed, near-surface flow behavior through the drag crisis was studied by Cheng *et al.* [2], who observed local mean-flow separation bubbles at both sub-critical and supercritical Re_D. The azimuthal variation of the skin-friction coefficient obtained from their LES agreed well with experiment [3]. Cheng *et al.* concluded that the occurrence of the drag crisis was strongly related to the interaction of the main separation shear layer with unsteady, secondary flow cells that reattach within the large-scale separation zone. They argued that boundary-layer laminar to turbulent transition is more likely a strong effect of the drag crisis rather than its primary causal agent.

When the cylinder is rotating about its axis with constant rotational speed Ω, the non-dimensional rotation speed $\alpha = \Omega D/(2U_\infty)$ is introduced as an additional flow parameter. That the lift coefficient C_L generally increases with increasing α at fixed Re_D was demonstrated in early experimental studies [4, 5]. When Re_D is fixed at values greater than about $Re_D = 3.58\times10^4$, Swanson [6] found experimentally that C_L suddenly decreased and subsequently continued to increase as α passed through a small band whose lower and upper bounding values were dependent on Re_D. This has become known at the lift crisis. Subsequent experiments [7, 8] confirmed this effect. The lift crisis, also referred to as the inverse Magnus effect, has also been observed for flow over a rotating sphere where the axis of rotation is orthogonal to the direction of the free stream [9].

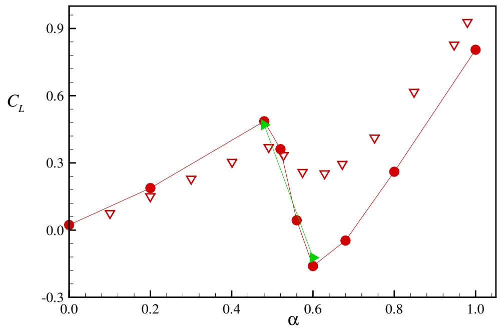

Figure 1: The lift crisis phenomenon viewed by varying α at fixed $Re_D = 6\times10^4$. Hollow symbols: experiment by Swanson [6]. Filled symbols: LES data.

Case	Re_D	N_θ	N_r	N_y
A1	5×10^3	512	256	96
B1	1×10^4	512	256	96
C1	2×10^4	512	256	96
D1	4×10^4	2048	256	192
E1	6×10^4	2048	256	192
F1	8×10^4	2048	256	192
G1	1×10^5	2048	256	192

Table 1: Fixing $\alpha = 0.6$ and varying Re_D.

Cheng *et al.* [10] implemented wall-resolved large-eddy simulation at two Re_D with α in the range $0 \le \alpha \le 1.0$. At their low $Re_D = 5\times10^3$, a lift crisis was not found. At $Re_D = 6\times10^4$, profiles of both pressure coefficient C_p and skin-friction coefficient $C_{f\theta}$ clearly illustrate the presence of a lift crisis in $0.48 \le \alpha \le 0.6$. This range agrees well with experimental data [6]. Presently, we report results obtained from LES of flow over a cylinder with increasing Re_D at $\alpha = 0.6$ fixed. This will be shown to provide both an alternative view of the lift-crisis behavior, and will also give insight into the scaling of the azimuthal component of the surface skin-friction vector with Re_D for a rotating cylinder flow.

LES performed

In Cartesian (x,y,z) co-ordinates, we describe LES of flow in the x direction about a cylinder rotating about the y-axis. The governing LES equations are solved numerically in time and space using a fourth-order accurate central-difference method where the skew-symmetric form of the convection term is discretized by an energy-conservative scheme. A standard fractional-step method is combined with a third-order Runge-Kutta method for time integration. A multigrid solver with line-relaxed Gauss-Seidel smoothing is utilized for solution of the

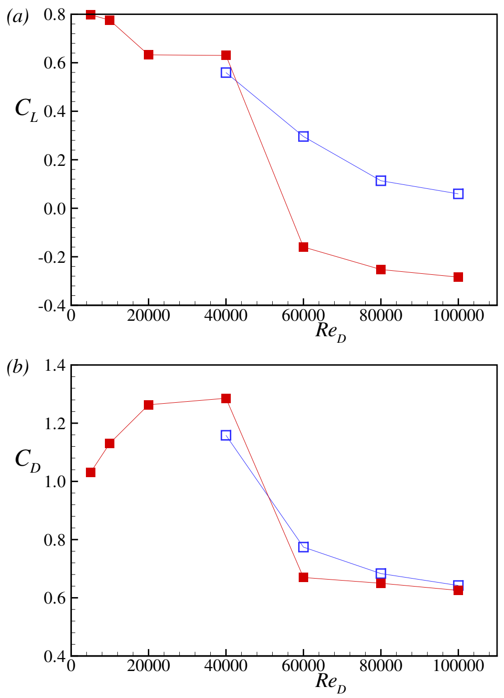

Figure 2: Fixing $\alpha = 0.6$ and varying Re_D. (a): C_L; (b): C_D. □, experiments by [8]; ■, present LES.

Helmholtz equations for velocity and the Poisson equations for pressure.

In the present LES, unresolved subgrid motions are represented by the stretched-vortex (SV) sub-grid scale model [11]. In cylindrical (r, θ, y) co-ordinates, the computational domain is a body-fitted O-grid with $L_r = 40D$ and $L_y/D = 3.0$. Grid spacing is uniform in the θ and span-wise y-directions but is stretched in the r direction. At the wall, a non-slip boundary condition is applied while the wall-normal grid resolution is of order the local viscous length scale ν/u_τ where $u_\tau = \sqrt{\tau_w/\rho}$ is the local friction velocity and τ_w the local shear stress. Hence the LES is considered wall-resolved. The code has been verified in previous studies by comparison with DNS [2, 10].

The cylinder rotation is clockwise when viewed in the positive y direction and the co-ordinate θ is taken as increasing clockwise with $\theta = 0$ on the negative x-axis. The "top" of the cylinder is then at $\theta = 90^o$, where the movement direction of the cylinder surface is parallel to the free stream while the "bottom" of the cylinder is $\theta = 270^o$, where the cylinder surface moves anti-parallel to the free stream. A range of LES were performed with different resolution (N_r, N_θ, N_y), as shown in table 1 where $Re_D = 5 \times 10^3 - 10^5$. All flows have $\alpha = 0.6$.

Results

Lift and drag coefficients C_L, C_D

Figure 1 shows LES results for the lift coefficient (in z-direction) $C_L(\alpha)$ versus α at fixed $Re_D = 6 \times 10^4$ [10] . In $0.48 \le \alpha \le 0.6$, both the data of Swanson [6] and the LES show a lift crisis in the form of a sudden decrease of C_L followed by recovery and subsequent increase. The local maximum $\rightarrow$ local minimum drop in C_L given by the LES substantially exceeds that indicated by experiment. Swanson [6] does not give extensive details of the experimental technique. Experiments of flow past a rotating sphere [9] show a strong lift crisis with negative C_L at comparable Re_D to the present LES.

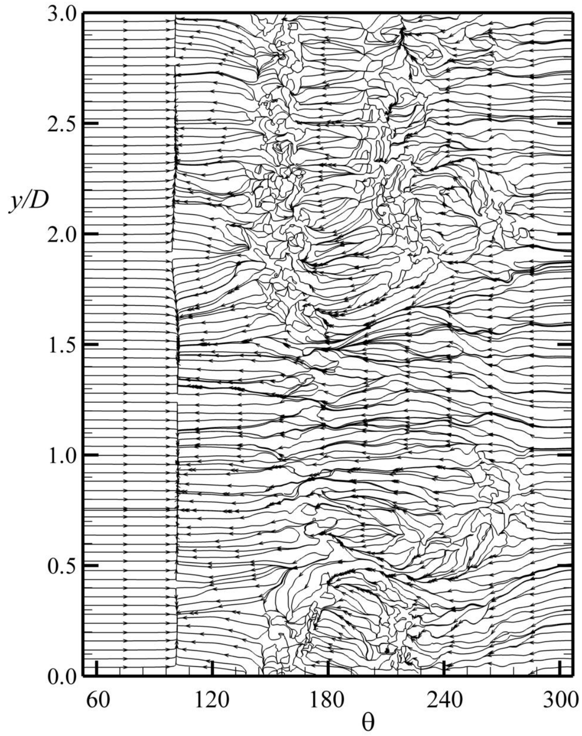

Figure 3: Skin friction lines at a time instant during a typical $C_L(t)$ cycle at $Re_D = 4 \times 10^4$, $\alpha = 0.6$ before the lift crisis.

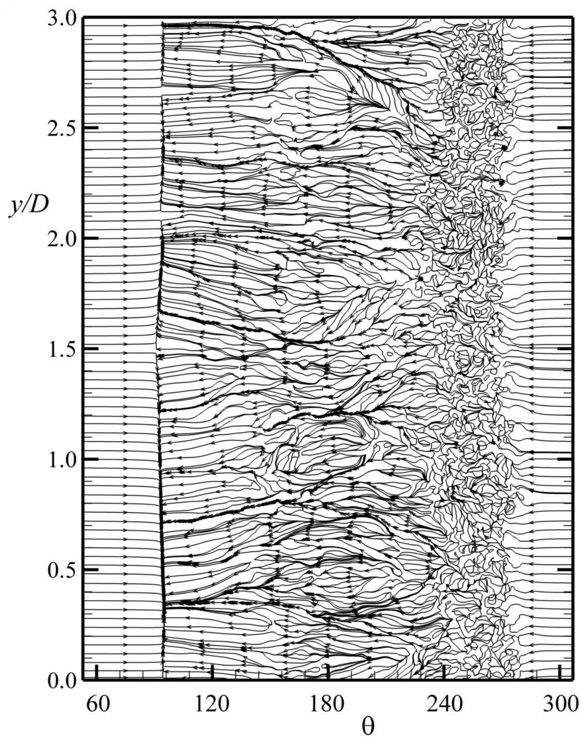

Figure 4: Skin friction lines at a time instant during a typical $C_L(t)$ cycle at $Re_D = 6 \times 10^4$, $\alpha = 0.6$ after the lift crisis.

The variation of $C_L(Re_D)$ and $C_D(Re_D)$ with Re_D for $\alpha = 0.6$ are shown in figure 2. In figure 2(a), the present LES shows a quite sharp decrease in C_L over the range $4\times10^4 \le Re_D \le \times10^4$. Experimental values [8] show a more moderate decline but over a similar range of Re_D. Both experiment and the present LES shows a substantial decrease in C_D over $4\times10^4 \le Re_D \le 6\times10^4$. This drag crisis, corresponding to a 50% reduction in C_D, is not as strong as that experienced by the non-rotating cylinder flow (at much larger Re_D).

Cylinder surface skin-friction portraits

To investigate the surface flow features before and after the lift crisis, we show plots of instantaneous skin-friction lines. These correspond to direction-field portraits of the surface skin-friction vector field $\mathbf{C}_f(\theta, y, t)$ on the developed cylinder surface. While the details of these plots show some variation during a typical vortex shedding or $C_L(t)$ cycle at any given (Re_D, α), structural changes in general features of the portraits as Re_D is increased at fixed α, can provide insight into flow separation events through the lift crisis. Figure 3 shows a portion in $(55^\circ \le \theta \le 305^\circ, 0 \le y/D \le 3.0)$ of a typical instantaneous $\mathbf{C}_f(\theta, y, t = \text{const})$ image at $Re_D = 4\times10^4$, $\alpha = 0.6$ prior to the lift crisis. The separatrix corresponding to the primary shear layer separation is clearly visible at $\theta \approx 95-100^\circ$. At larger θ patches of scattered, small-scale separation/reattachment cells can be see as indicated by the presence of critical points of the $\mathbf{C}_f$ field. These events co-exist with regions of coherent, nearly uniform flow in the anticlockwise direction. This mixing of local separation and attached, near-surface back flow is sufficiently strong to form both wall-attached and fully-separated vortices [10].

When $Re_D = 6\times10^4$, $\alpha = 0.6$ after to the lift crisis, figure 4 shows a transition to a more ordered state where the small-scale separation/reattachment cells have aggregated into a narrow band in $230^\circ \le \theta \le 270^\circ$ that is coherent across the whole span. This indicates the presence of strong, highly localized near-surface vorticity associated with the formation of a local deep pressure minimum (see figure 5). Apart from primary separation on the top cylinder surface, the flow is largely attached elsewhere. This sudden transition in surface separation patterns is the dynamical signature of the list crisis. We have shown that it is invariant when viewed either at fixed Re_D with increasing α [10] or conversely with fixed α with increasing Re_D.

Pressure coefficient C_p and skin friction coefficient $C_{f\theta}$

Distributions of span-wise and time-averaged $C_p(\theta)$ are shown in figure 5. The variation of $C_p(\theta)$ is similar for both $Re_D = 5\times10^3, 10^4$ (figure 5(a)) including a minimum region around the top side of the cylinder and a plateau value of $C_p \approx -1$ on the rear or leeward side of the cylinder. At higher $Re_D = 2\times10^4, 4\times10^4$, the plateau decreases to about $C_p \approx -1.3$. Further increase in Re_D leads to substantial changes in $C_p(\theta)$. For $Re_D = 6\times10^4$, shown in both figures 5(a) and 5(b), the minimal C_p on the top side of the cylinder is increased markedly while the plateau region is shifted to about $C_p \approx -0.7$. On the bottom side of the cylinder, where the cylinder motion opposes the free-stream velocity, a sharp decrease in the C_p minimum at about $\theta = 270^\circ$ can be observed. This change gives rise to the lift crisis. As shown in figure 5(b), further increase in Re_D does not produce substantial changes in $C_p(\theta)$ distributions.

Corresponding distributions of the azimuthal coefficient of the skin-friction $C_{f\theta}$ are shown in figure 6. The subfigures 6(a)/6(b) show Re_D below/above the lift crisis, respectively, except that $Re_D = 6\times10^4$ is shown in both plots. For these distributions, in addition to the monotonic decrease of the peak $C_{f\theta}$

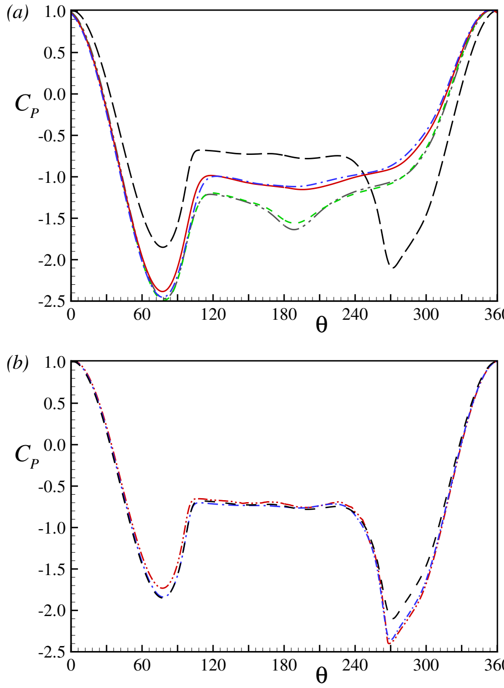

Figure 5: $\alpha = 0.6$. Pressure coefficient $C_p(\theta)$. (a): —·— , $Re_D = 5\times10^3$; ——— , $Re_D = 1\times10^4$; - - - - , $Re_D = 2\times10^4$; —··— , $Re_D = 4\times10^4$; — — — — , $Re_D = 6\times10^4$. (b): — — — — , $Re_D = 6\times10^4$; —·— , $Re_D = 8\times10^4$; ——— , $Re_D = 1\times10^5$.

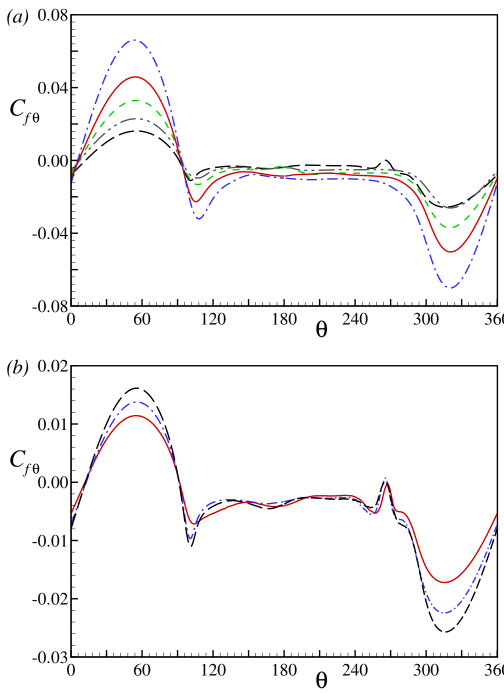

Figure 6: $\alpha = 0.6$. Skin friction coefficient $C_{f\theta}(\theta)$. (a): —·— , $Re_D = 5\times10^3$; ——— , $Re_D = 1\times10^4$; - - - - , $Re_D = 2\times10^4$; —··— , $Re_D = 4\times10^4$; — — — — , $Re_D = 6\times10^4$. (b): — — — — , $Re_D = 6\times10^4$; —·— , $Re_D = 8\times10^4$; ——— , $Re_D = 1\times10^5$.

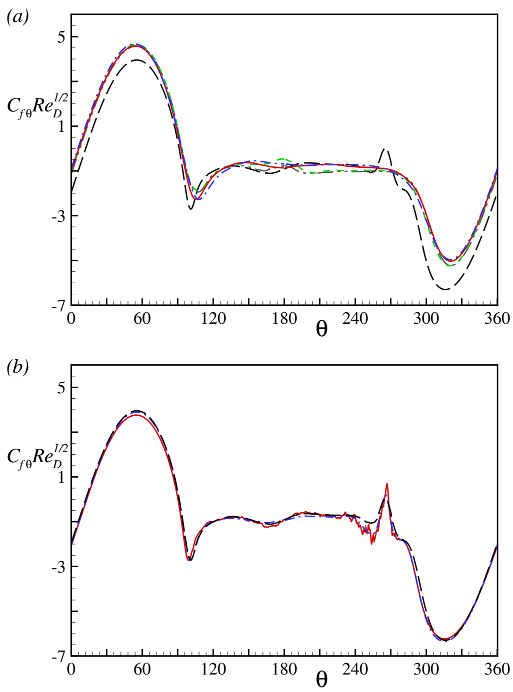

Figure 7: $\alpha = 0.6$. Scaled skin friction coefficient. (a): — · —, $Re_D = 5\times10^3$; ——— , $Re_D = 1\times10^4$; - - - - , $Re_D = 2\times10^4$; — · · — , $Re_D = 4\times10^4$; — — — — , $Re_D = 6\times10^4$. (b): — — — — , $Re_D = 6\times10^4$; — · — , $Re_D = 8\times10^4$; ——— , $Re_D = 1\times10^5$.

at around $\theta = 60$ with increasing Re_D, the main effect of Re_D is the appearance of a small local maximum or "hill" at about $\theta = 270^\circ$. This is absent for $Re_D \leq 4\times10^4$, but is observed for $Re \geq 6\times10^4$.

For over a cylinder with $\alpha = 0$ Cheng *et al.* [2] found evidence that the scaled skin-friction $C_{f\theta}(\theta)\,Re_D^{1/2}$ showed good collapse independent of Re_D with a peak value $C_{f\theta}Re_D^{1/2} \approx 5$. In figure 7, we show $C_{f\theta}(\theta)\,Re_D^{1/2}$ for varying Re_D with $\alpha = 0.6$. Here also, subfigures 7(a)/7(b) show distributions for Re_D below/above the lift crisis, respectively, except that $Re_D = 6\times10^4$ is common to both plots.

It is evident that, for the range of Re_D shown, there is good collapse of $C_{f\theta}(\theta)\,Re_D^{1/2}$ for both subcritical and for super-critical Re_D, but that the collapse lines are rather different for the two Re_D ranges. For $Re_D \leq 4\times10^4$, the peak scaled skin friction on the top side of the cylinder reaches $C_{f\theta}Re_D^{1/2} \approx 4.8$ while on the bottom side we find a minimum $C_{f\theta}Re_D^{1/2} \approx -5$. For $Re_D \geq 6\times10^4$, the peak on the top side decreases to about $C_{f\theta}Re_D^{1/2} \approx 4$ and the corresponding bottom side decreases to about $C_{f\theta}Re_D^{1/2} \approx -6.5$. We conclude that at constant $\alpha = 0.6$, the scaling $C_{f\theta}(\theta)\,Re_D^{1/2}$ remains valid, but separate, over subcritical and supercritical Re_D.

Conclusion

Large-eddy simulation has been used to investigate the lift crisis phenomenon in high Reynolds number rotating cylinder flows. With $\alpha = 0.6$, our LES captures a decrease of C_L from $Re_D = 4\times10^4$ to 6×10^4. Instantaneous skin friction lines are used to reveal changes in flow separation that occur as Re_D passes through the lift crisis. Changes in the surface skin-friction portraits are found to be essentially the same as those observed when the lift crisis is viewed at fixed α but with increasing Re_D. The common underlying mechanism is characterized by a change in surface-separation structure, on the leeward and bottom cylinder surface, from scattered separation cells to near-wall, small-scale reversal flows aggregating into a relatively narrow azimuthal zone. This produces both small-scale incoherent separation and a strong pressure minimum. The scaling of the skin friction as $C_{f\theta}(\theta)\,Re_D^{1/2}$ is found to work quite well at $\alpha = 0.6$.

Acknowledgement

The Cray XC40 Shaheen at KAUST was used for all simulations reported.

References

[1] O. Lehmkuhl, I. Rodriguez, R. Borrell, J. Chiva and A. Oliva. Unsteady forces on a circular cylinder at critical Reynolds numbers. *Phys. Fluids* **26**, 4904415, 2014.

[2] W. Cheng, D.I Pullin, R. Samtaney, W. Zhang, and W. Gao. Large-eddy simulation of flow over a cylinder with Re_D from 3.9×10^3 to 8.5×10^5: a skin-friction perspective. *J. Fluid Mech.* **820**, 121–158, 2017.

[3] E. Achenbach. Distribuion of local pressure and skin friction around a circular cylinder in cross-flow up to Re=5×10^6. *J. Fluid Mech.* **34**, 625–639, 1968

[4] E.G Reid. Tests of rotating cylinders. *Tech. Rep.* No. 209. National Advisory Committee for Aeronautics, 1924.

[5] A Thom. Experiments on the flow past a rotating cylinder. *Aeronautical Research Committee, Reports and Memoranda* 1410, 1931.

[6] W.M. Swanson The Magnus effect: A summary of investigations to date. *Journal of Basic Engineering* **83**, 461–470, 1961.

[7] C.A Fletcher. Negative Magnus forces in the critical Reynolds number regime. *J. Aircraft* **9**, 826–834, 1972.

[8] S. Takayama, and K Aoki. Flow characteristics around a rotating grooved circular cylinder with grooved of different depths. *Journal of Visualization* **8**, 295–303, 2005.

[9] J. Kim., H. Choi, H. Park and J.Y. Yoo Inverse Magnus effect on a rotating sphere: when and why, *J. Fluid Mech.* **754**, R2, 2014

[10] W. Cheng., D. Pullin, R. Samtaney Large-eddy simulation of flow over a rotating cylinder: the lift crisis at $Re_D = 6\times10^4$, *J. Fluid Mech.* **855**, 371–407, 2018

[11] A. Misra, A. and D. I. Pullin. A vortex-based subgrid stress model for large-eddy simulation. *Phys. Fluids* **9**, 2443–2454, 1997